Multiple phases of $Cu_2ZnSnSe_4$ detected by room temperature photoluminescence

Rabie Djemour, Alex Redinger, Marina Mousel, Levent Gütay, and Susanne Siebentritt

Citation: Journal of Applied Physics **116**, 073509 (2014); doi: 10.1063/1.4892101
View online: http://dx.doi.org/10.1063/1.4892101
View Table of Contents: http://aip.scitation.org/toc/jap/116/7
Published by the American Institute of Physics

Multiple phases of $Cu_2ZnSnSe_4$ detected by room temperature photoluminescence

Rabie Djemour, Alex Redinger, Marina Mousel, Levent Gütay,[a] and Susanne Siebentritt[b]
Laboratory for Photovoltaics, Physics and Materials Science Research Unit, University of Luxembourg, 4422 Belvaux, Luxembourg

(Received 24 April 2014; accepted 23 July 2014; published online 21 August 2014)

$Cu_2ZnSnSe_4$ based solar cells are promising but suffer from low open circuit voltage relative to their band gap. Additionally, the bandgap as extrapolated from quantum efficiency (QE) measurements varies without clear correlation to the growth conditions. Using room temperature photoluminescence, we show that different materials with different bandgaps coexist within micrometer sized areas of the absorbers. Simulations of the effect of multiple bandgaps on both the absorption and the Shockley-Queisser radiative recombination limit, explain the variations of the bandgap extrapolated from QE and the deficiencies of the solar cell parameters. © *2014 AIP Publishing LLC*.
[http://dx.doi.org/10.1063/1.4892101]

I. INTRODUCTION

$Cu_2ZnSn(S/Se)_4$ (CZTSSe) and related compounds are being investigated as an alternative to the current thin film solar cell technologies. The resulting solar cells have shown rapid improvement.[1,2] However, these cells still underachieve in the open circuit voltage (V_{oc}) which leads to lower efficiencies compared to the closely related $Cu(In,Ga)Se_2$ thin film solar cells.[3,4] Open circuit voltage losses are recombination losses and consequently the nature of these losses has to be studied in detail in order to improve the solar cell efficiencies. Up to now, low open circuit voltages in CZTSSe based solar cells have been assigned to dominant interface recombination and/or low minority carrier lifetimes.[5,6] However, in pure selenide CZTSe solar cells the open circuit voltage losses cannot be attributed to interface recombination.[6] The minority carrier lifetimes have been reported to be only of a few nanoseconds.[7]

In this paper, we will focus on pure selenide CZTSe absorbers and their solar cells. One important aspect has only been rarely discussed: Even the best performing CZTSe devices show a rather poor low-energy response in the quantum efficiency curves (QE).[6–9] Moreover, a significant scatter in the bandgaps extracted from QE (i.e., from 0.8 eV to 1 eV) can be observed for nominally the same material.[6–9]

The bandgap can also be extracted from room temperature photoluminescence (RT-PL). While short range band gap fluctuations, e.g., because of alloy disorder, shift the PL maximum below the band gap[10] the PL maximum is still a measure for the band gap energy. The PL spectra in the currently best performing CZTSe devices peak at different energies: 0.96 eV (Ref. 7) in coevaporated samples, 0.86 eV, 0.93 eV, and 1.02 eV in coevaporated and annealed samples,[9] 0.91 eV in samples from a sequential process with coevaporated precursors,[11] around 0.85 eV and around 0.92 eV in samples from a sequential process with sputtered precursors.[12] The PL spectra often show one dominant transition together with one or several shoulders or additional smaller peaks at slightly lower or higher energies. In some cases, only one transition is observed which is then very broad and asymmetric. Shin *et al.*[9] observed several transitions ranging from 0.86 eV up to 1.02 eV depending on the growth parameters. They attributed the different PL transitions to defect transitions which vary with the Se content during annealing. Brammertz *et al.*[12] observed PL transitions ranging from 0.85 eV to 0.92 eV which they also attribute to defect related transitions, varying with a Sn gradient in the films.

We propose an alternative explanation of the different PL maxima and attribute the PL transitions to band to band transitions. This implies that different materials coexist in one absorber layer. This coexistence is probable in CZTSe since it has a small existence region easily leading to secondary phases[13–15] and has a multitude of polymorphs (kesterite, stannite, disordered kesterite) that have been predicted to have different bandgaps.[14–16] The presence of secondary phases in CZTSe can, to a certain extent be checked using Raman spectroscopy.[17,18] It is a tougher task to distinguish the different polymorphs. So far, only neutron scattering techniques can discern the different polymorphs of CZTS/Se.[19] Raman scattering can confirm the presence of kesterite in the CZTS[20,21] and CZTSe[22] absorbers but cannot exclude that other polymorphs are present in the sample.

We show in this contribution that RT-PL can be used to confirm the presence of different phases (either secondary phases with different composition or polymorphs of CZTSe) with various bandgaps in the absorber. The RT-PL measurements show the luminescent recombination involving either only the bands, or the band and the deep defects.[23] When the sample is at room temperature PL is not expected from shallow defects and excitons. Shallow defects do not show luminescent transitions at room temperature since they are thermally emptied. The same is true for excitons: most materials have exciton binding energies far below the thermal energy at room temperature. Excitons have been observed in

[a]Current address: Energy and Semiconductor Research Laboratory, Institute of Physics, Carl von Ossietzky University, 26111 Oldenburg, Germany.
[b]susanne.siebentritt@uni.lu

CZTSe[24] and in CZTS[25] by low temperature PL; both materials show rather high energy excitonic emissions, which quench very quickly with increasing temperature, indicating low exciton binding energies. Therefore, we have chosen to study the PL at room temperature, since it provides us with the possibility to distinguish between transitions emerging from different bandgaps.

Monitoring the evolution of the PL signal intensity with the excitation laser intensity (P) allows conclusions on the nature of the examined transition. The PL signal intensity for a given energy is proportional to the PL yield (Y_{PL}). The luminescence yield follows a power law: $Y_{PL}(P) = P^k$; where k is a characteristic parameter for the transition.[26,27] Y_{PL} is proportional to the density of involved charge carriers: for a band-band transition $Y_{PL} \propto n \cdot p$; where n is the density of free electrons and p is the density of free holes. In our measurement conditions, we have to consider high injection (i.e., the number of charge carriers in thermal equilibrium is negligible compared to the injected charge carriers), band to band transitions then have a k of 2 as free electron and free hole densities n and p are each proportional to the excitation intensity. One could argue that for recombination in an ideal semiconductor for every photon "in" only one photon can come out. However, no semiconductor is ever ideal, particularly not the ones we are discussing here, therefore each excited charge carrier pair has a probability considerably smaller than 1 to recombine radiatively. Therefore, we have to consider the probability of an electron to recombine with a hole, and this probability is proportional to $n{\cdot}p$, resulting in an exponent in the power law of 2. For defect-band transitions, we expect $Y_{PL} \propto n$ or $Y_{PL} \propto p$, since the other type of charge carrier is determined by the defect density which leads to: $k = 1$. These k values are diminished from their ideal values of 1 or 2 by competing non-luminescent recombination paths which results in $k < 1$ for defect-band transitions and $k < 2$ for band-band transitions (see Ref. 27, chapter 7 in Ref. 23, chapter 7 in Refs. 28 and 26).

Thus, at room temperature, we can only expect as radiative recombination channels band-band transitions or defect related transitions, involving rather deep defects. A donor-acceptor pair transition can be easily distinguished, as it blue shifts with increasing excitation intensity.[23,28] A defect-band transition will never have an exponent larger than 1 since it only depends on the free electron density or on the free hole density.[26] A band-band transition has generally (however not necessarily) an exponent larger than 1. Therefore, an exponent larger than 1 is a clear indication of a band-band transition and cannot be related to a defect-band transition.

We show here that the RT-PL spectra show several transitions with $k > 1$, i.e., several materials with different bandgaps. A similar conclusion has been drawn from low temperature PL measurements of Cu_2ZnSnS_4.[29] The effect of these materials with different bandgaps on the solar cell parameters will be elucidated. A simple analytical model is presented which shows how different bandgaps influence the quantum efficiency spectra. Additionally, we calculate the influence of different materials with different bandgaps on the Shockley Queisser (SQ) limit, which considers the case of an ideal solar cell in order to illustrate the detrimental effect on device performance.

II. EXPERIMENTAL

The samples are prepared by the simultaneous deposition of all elements by co-evaporation followed by an annealing in the presence of Se and SnSe powder to prevent CZTSe decomposition.[30] The final composition of all samples is Cu poor ($Cu/(Zn + Sn) < 1$) and Zn rich ($Zn/Sn > 1$). Compositions are measured by energy dispersive X-ray spectroscopy (EDX) in an electron microscope. The precursors used are Cu-poor or Cu-rich and etched, as discussed in the paper of Mousel *et al.*[31] The efficiencies of the discussed solar cells are between 4% and 7%. We observe the luminescence features, which we discuss in this paper, in all samples, independent of the details of the CZTSe absorber preparation process. We see the same features in samples where the precursor were deposited by electrodeposition (these samples are not discussed in this paper). Also the details of the annealing are not important. The same features are observed in samples annealed in a tube furnace (at 450 °C–550 °C) or in set-up for rapid thermal processing (RTP at 550 °C). As we discuss later, similar effects are also observed in various PL spectra presented in the literature. The PL spectra we report here are measured on blank absorbers. The solar cells were made from another piece on the same substrate, after breaking the substrate into different pieces.

The quantum efficiency (QE) was measured using a home built setup equipped with lock-in technique.

The RT-PL measurements have been carried out on the CZTSe absorbers in a confocal home-built setup also capable of performing Raman measurements. An argon ion laser provides the 514.5 nm laser radiation which is used as excitation source. The laser intensity is set by adjusting the output power of the laser. The actual light intensity which proceeds through the optical setup is measured by a powermeter. The laser beam is focused by means of a microscope lens which results in a spot size of about 1 μm in diameter. A more detailed description of the setup can be found in Ref. 17. The injected charge carrier densities are estimated to be $4 \times 10^{17}\,cm^{-3}$ for the lowest used excitation intensities of about 0.01 mW, assuming 500 nm penetration depth, and 10 ns carrier lifetime. This is consistent with high injection mode since the doping densities for working solar cells have to be less than $5 \times 10^{16}\,cm^{-3}$.[32]

For the intensity dependent PL study presented here, the absorber layers have been etched with a 0.02 M Br_2-methanol solution in order to remove potential oxide layers on top of the absorber. This etching does not affect the PL transitions, i.e., the transitions and intensity behaviours shown are also seen on unetched samples.

III. RESULTS AND DISCUSSION

A. RT PL shows multiple materials

PL spectra observed on CZTSe in both our lab and in the literature vary quite a lot in PL peak position and shape.

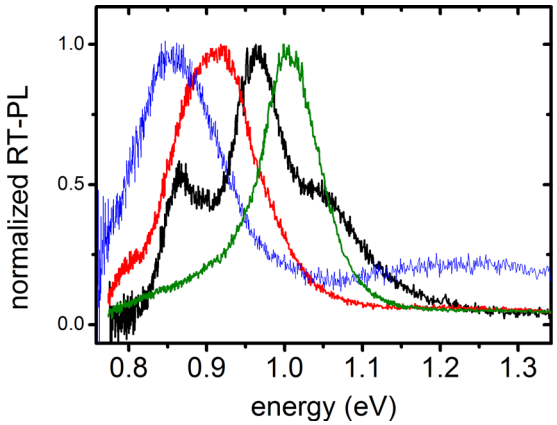

FIG. 1. Green excitation photoluminescence spectra measured on CZTSe absorbers normalized for a better overview.

This effect is demonstrated in Fig. 1 which depicts a variety of PL spectra of a number of similar CZTSe films. The PL transitions we present in Fig. 1 show the range of different PL spectra seen on CZTSe samples that are made in the Cu-poor Zn-rich composition, and give decent solar cells (usually between 4% and 7% conversion efficiency). More than 10 samples have been analyzed by PL. Fig. 1 shows the variation in the spectra. The PL spectra were similar to the ones shown in Fig. 1 or combinations thereof, see Fig. 2(a) for an example of a combination.

It should be noted that all the measurements discussed in this paper are PL measurements made on a micrometer sized spot. This leads to the fact that the spectra of macroscopic measurements, usually shown in literature, tend to be broader, smeared out since they average the inhomogeneities that might be present in the sample.

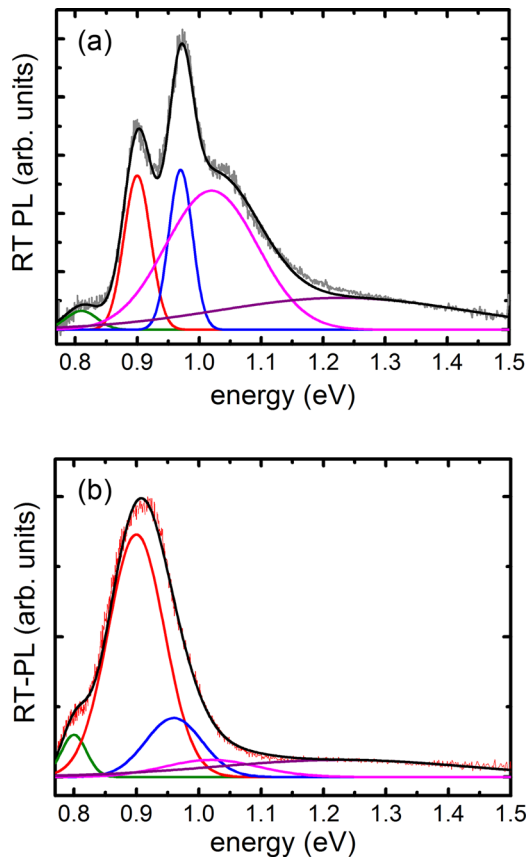

FIG. 2. RT-PL spectra fitted using multiple Gaussians. (a) Shows a fit from the intensity dependent study. (b) Shows the fit of the red curve of Fig. 1.

All these absorbers give working solar cell devices, see Table I. Although solar cells which have a dominant luminescence around 0.82 eV, like the blue curve in Fig. 1, tend to have a lower open circuit voltage, no clear correlation between the PL spectra and the efficiency of the corresponding solar cells can be detected. It should also be taken into account that the PL spectra shown here are all taken at or near the surface of the absorber. In some cases, we have sputtered into the absorbers to different depths and measured PL at the bottom of the sputter crater. We find that the PL spectra change with depth.[17,31] All absorbers discussed here show a very similar composition and very similar Raman spectra, as discussed in Ref. 22. Therefore, we analyse these PL spectra under the assumption that these absorbers are composed of similar materials. Clearly, their main phase is $Cu_2ZnSnSe_4$. Based on the Raman analysis discussed in detail in Ref. 22, we can conclude that the main polymorph is kesterites. However, the absorbers can certainly contain the stannite phase to a smaller amount, which has a lower bandgap. A third possible phase is another polymorph with the same composition, based on Cu-Au ordering, which has been predicted with an even lower bandgap.[14] Disordered kesterite[19] is another possible phase, no predictions on the band gap are available. In addition secondary phases can exist, like ZnSe, SnSe, $SnSe_2$, Cu_2SnSe_3, and other CuSn-selenides or various Cu-selenides. All these different phases and crystal modifications will have different bandgaps and different defect energies and will therefore show emissions at different energies. The intensity of each emission does not necessarily correlate with the amount of material present since the PL intensity strongly depends on the ratio of radiative to non-radiative recombination in each material, as well as on charge carrier diffusion processes between materials.

Based on the assumption that the various absorbers are similar, we fit the different spectra with the same number of peaks with fixed energetic positions, allowing in general for a 20 meV shift. It can be reasonably assumed that the various samples do not consist of hundreds of different materials and furthermore will not exhibit hundreds of different band gaps. The sample depicted in Fig. 2(a) clearly shows four distinct peaks in the energy region of the kesterite band gap. We show later that all four observed transitions around the expected kesterite band gap are band-band transitions. Therefore, we tested if we can use those four emission energies for all samples. By the fact that this is possible, as

TABLE I. Solar cell parameters of PL samples.

PL of sample	η/%	V_{OC}/mV	j_{SC}/mAcm^{-2}	FF/%
Fig. 1: blue	2.0	240	21	40
Fig. 1: red	7.5	356	35	60
Fig. 1: black	5.1	325	29	54
Fig. 1: green	6.2	353	34	52
Fig. 2(a)	5.5	333	32	52

shown exemplary in the following, we believe that there are four different materials in our samples, with differing relative amounts. In some samples, there are only one or two of these materials, leading to a single, maybe broadened peak. Examples for such fits are shown in Fig. 2. The spectrum in Fig. 2(b) could of course be fitted with only three peaks, with different energies than the emissions observed in Fig. 2(a). But if we assume that the materials in our absorbers are more or less the same, the PL emission should show maxima at the same energies, allowing for small shifts due to strain or defects. It turns out that a large number of PL spectra of different samples, as well as PL spectra from the literature,[7,9] can be fitted with 5 peaks with fixed energies.

We use Gaussians to fit the PL peaks. Whilst this is reasonable for defect related transitions in a (somewhat) disordered environment, for band-band transitions one would expect a shape determined by the generalised Planck's law.[33,34] However, this requires the knowledge of the absorption spectrum, particularly when the semiconductor does not show a sharp absorption edge but strong tailing, as is usually the case in kesterites, see also Fig. 5. Therefore, for a band gap that is affected by strong tailing we need to find a function that does not require any a priori knowledge. The peaks in Fig. 1 appear almost symmetrical and can be well fitted by Gaussians, see Fig. 2. Therefore, we use Gaussians to fit all peaks.

All the measured RT PL spectra have their transition maxima at energy positions similar to those shown in Fig. 1 or can be deconvoluted using the same distinct peak positions, see Fig. 2. Depending on the measured sample these peak positions usually are shifting within 0.02 eV: The distinct peak positions we find fitting the vast majority of our samples are (0.83 ± 0.03) eV, (0.90 ± 0.01) eV, (0.96 ± 0.01) eV, and (1.02 ± 0.01) eV. The errors are given by the extremal values of all fitted positions where only two outlier measurements are discarded. The peak at higher energy varies between 1.2 eV and 1.4 eV and is related to a ZnSe secondary phase, as demonstrated previously.[17] The full width at half maximum for the ZnSe PL is high (up to 0.4 eV) while for the lower energy peaks it is around 0.15 eV for the 1.02 eV peak and around 0.04 eV (up to 0.09 eV for some samples) for all other lower energy peaks. As an example for fitting samples that appear different but can still be deconvoluted with the same peaks we present the fit of the red curve in Fig. 1, as depicted in Fig. 2(b).

The intensity ratio of the various peaks cannot be correlated with the composition or the Raman spectra of the samples. Also within one sample we cannot detect any correlation between the maps of the various PL peaks and any feature in the Raman spectra, besides for the ZnSe peak, as discussed in Ref. 17.

To study whether the observed emissions can be due to defect related transitions or due to band-band transitions, we have checked the dependence of the emission intensities and energetic positions on the laser excitation intensity. The peak energies do not shift with excitation power, thus we can exclude a donor-acceptor pair transition. For the intensity of the emission, we expect a power law as discussed above. One sample shows all 5 transitions simultaneously in a particularly well resolved way, see Fig. 2(a). It permits therefore to measure the power laws of all the transitions at once.

Fig. 3 shows a double logarithmic plot of the evolution of the RT-PL peak intensity as a function of the excitation laser power for the sample shown in Fig. 2(a), where we show the spectrum with 2 mW excitation power as an example. The PL intensities are fitted using Gaussian peak shapes. Since the peak widths do not change with excitation intensity we keep them constant in the fit. Therefore, the change of the intensity can be taken from the maximum or the peak area. The k value is then given by the slope of the linear fit between PL intensity and excitation intensity in the double logarithmic plot.

The luminescence at 1.2 eV is attributed to a ZnSe secondary phase in accordance with previous findings.[17] This PL emission has a k value of 0.75 indicating a defect related transition which confirms the attribution of this transition to a defect related transition in ZnSe.[17]

The k values of the PL transitions at 0.82 eV, 0.9 eV, 0.97 eV, and 1.02 eV are all higher than 1. In various samples, where one of these peaks dominates, we find the same result: All 4 low energy emissions have an exponent larger than 1. Since defect related transitions always show an exponent smaller than 1, the observation of $k > 1$ clearly indicates that these 4 observed transitions are band-band transitions. This suggests that different materials, i.e., different crystal polymorphs or secondary phases, are present in the sampled volume. The only alternative explanation for an exponent larger than 1 would be an excitonic emission. Excitons have been observed in low temperature PL experiments with selenide kesterites[24] and sulphide kesterite.[25] In both cases, high exciton emission energies have been found, in particular, at 1.03 eV at 5 K in the selenide kesterites that we investigate here, indicating a low exciton binding energy, which means that these excitons are impossible to observe at room temperature. A bound exciton, bound to a deep defect that was not present in the samples that showed the exciton at low temperature could also show an exponent larger than 1. However, these samples are all highly defective and strongly compensated, as manifested by broad luminescence peaks even at low temperatures,[35–38] which were also observed for

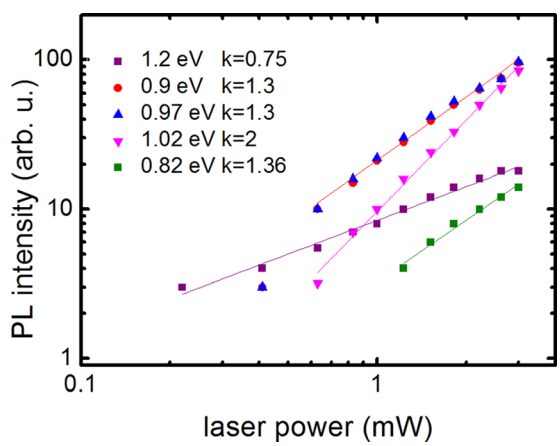

FIG. 3. Evolution of the fitted PL intensities as a function of the excitation laser intensity. A fitted PL spectrum for one laser power is shown in Fig. 2(a).

the samples considered here. It is very unlikely that an exciton can exist in such material. Therefore, the only remaining explanation for four different peaks with an exponent larger than 1 is the existence of four different materials with different band gaps. The fact that we observe all different peaks in 1 μm sized spot indicates that these materials are intimately mixed. One could expect that all the photogenerated carriers move to the material with the lowest gap and recombine there, making the lowest energy transition the most likely one, which is not what we observe. However, into which material the photogenerated charge carriers move depends on the band offsets. The electrons will tend to move to the material with the lowest conduction band edge, whereas the hole will move to the highest valence band edge, which could even lead to a spatial separation of charge carriers and suppress radiative recombination altogether. Additionally, the different materials are likely to show different doping levels, creating barriers at the interfaces. Therefore, even with closely intermixed materials the lowest energy transition is not at all the most likely one.

Although it is difficult to determine which polymorphs or secondary phases correspond to the different observed bandgaps, some possible phases can be excluded to a certain extend. As for the exclusion of secondary phases: SnSe and $SnSe_2$ are unlikely since they are not seen in the green excitation Raman spectra, measured on the same spot where the PL of Fig. 2(a) is measured, and shown in Fig. 4. The expected Raman modes for SnSe and $SnSe_2$ are shown in the figure. SnSe and $SnSe_2$ can be measured with Raman spectroscopy on our CZTSe solar cell absorbers under the same measurement conditions as shown in Ref. 18. Additionally, since our samples are grown in the Sn-poor composition range, Sn-selenides are not likely secondary phases. It also appears that Cu-selenides can be excluded as they have significantly higher bandgaps[39] than the energies of the observed emissions.

Therefore, we consider the most likely explanation for the different bandgaps the occurrence of various polymorphs of $Cu_2ZnSnSe_4$ and the occurrence of CuSn-selenide secondary phases. Various CuSn-selenides exist with bandgaps near the energetic region of the observed emissions: an orthorhombic low temperature (<450 °C) Cu_2SnSe_3 phase,[40] a monoclinic Cu_2SnSe_3 phase with a bandgap of 0.84 eV,[41] a cubic Cu_2SnSe_4 phase with a bandgap of 1.2 eV,[42] and a cubic Cu_2SnSe_3 phase.[43] No bandgaps were reported for the cubic and orthorhombic Cu_2SnSe_3. The monoclinic Cu_2SnSe_3 is a candidate to explain the emission at 0.82 eV. However, because of the lack of correlation with Raman data, we cannot conclude that this emission is due to the ternary phase. The bandgaps of various polymorphs of $Cu_2ZnSnSe_4$ have been calculated by different methods ranging from DFT (density functional theory) to GW.[14–16] Although there is no perfect agreement on the actual values of the bandgaps, all calculations find a difference of around 150 meV between the bandgaps of kesterite and stannite. The bandgap of the Cu-Au ordered structure is calculated to be another 30 meV below the bandgap of stannite.[14] These differences are in the range of the differences that we observe between the different emissions. Although we cannot definitely correlate the 4 emissions to a concrete polymorph or secondary phase, the important observation is that there are different materials present in the absorber, which have different bandgaps. This is certainly detrimental to the solar cells made from these absorbers, as we discuss in detail in the following.

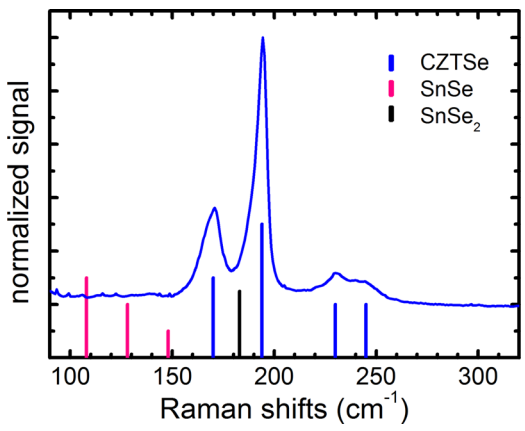

FIG. 4. Green excitation (514.5 nm) Raman spectrum measured on the sample used for the intensity dependent PL study shown in Figs. 2(a) and 3. The expected Raman modes for CZTSe,[22] SnSe, and $SnSe_2$[18] are indicated.

Remains the question how these materials are arranged within the film: in a columnar structure with different materials next to each other in the plane of the film, in a layered structure with the different materials on top of each other or in a three dimensional arrangement. Comparing spatially resolved PL spectra within each sample, we find similar spectra. Additionally, the spectra shown above were taken each on a 1 μm spot: within this spot we see the presence of different materials. While this observation could still be compatible with columns of a lateral extension much less than a micrometer, we find such needle like structure improbable based on the rather smooth structure seen in electron micrographs of all our kesterite films.[11,31,44] Thus, we rule out that the materials are arranged in a columnar fashion. To check for the appearance of a layered structure, we performed PL measurement in different depth of the film which were made accessible by sputtering craters of different depth into the film and we performed depth resolved SIMS (secondary ion mass spectroscopy) measurements. Both methods do not give any indication of the presence of different layers in the films. In some films, the surface composition or the composition near the back contact may be different from the composition of the majority of the film, as was observed before,[36,44] but none of the films showed a layered composition. We therefore conclude that the different materials must be 3-dimensionally intermixed, as was shown for the case of ZnSe in $Cu_2ZnSnSe_4$ films, prepared the same way, by atom probe tomography.[45]

B. Varying bandgap in QE

The bandgap can be approximated by a linear extrapolation of the low energy edge of the QE spectrum. Fig. 5 shows a selection of QE curves measured on samples with conversion efficiencies higher than 4%. The full QE spectra are shown in the inset. We use the approximately linear part of

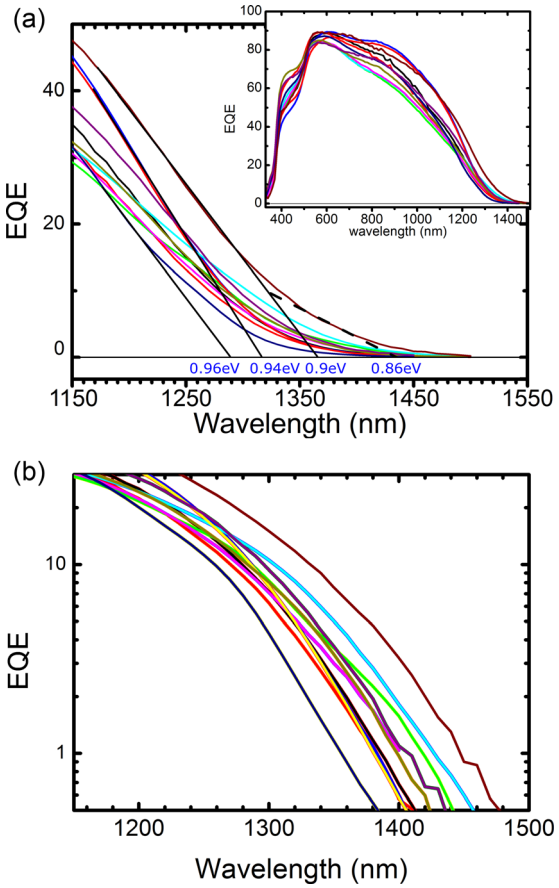

FIG. 5. QE measurements in the energy range of 1150 nm–1500 nm of CZTSe solar cells with conversion efficiencies higher than 4%. The blue lines show the linear extrapolations to the bandgap for three QE's (a). The inset shows the QE's in the full measured energy range (a). (b) Shows the same QE's in a logarithmic plot.

the QE spectrum in the range between about 10% and 40% QE for the extrapolation (as an example see the blue lines in Fig. 5). Other methods exist to determine the bandgap from QE measurements, all with their respective advantages and drawbacks. We chose the linear extrapolation since it is simple and does not depend strongly on the transport properties of the absorber. The bandgaps approximated this way vary between 0.9 eV and 0.96 eV, i.e., between the central two energies, which we observe in the PL spectra of the same absorbers. Some samples show a strong tailing towards lower energies. This tailing can be attributed to Urbach tailing or to a lower band gap material. Plotting the QE measurements in a logarithmic plot (depicted in Fig. 5(b)) shows that the low energy edge of the QE is linear in this plot which favours the attribution of the tailing to a strong Urbach tailing over its attribution to a lower band gap material, although based on the PL observation of a lower band gap material, we cannot draw a final conclusion on the tailing. Why we never see the energy of the lowest and the highest PL peaks in the edges of the QE spectra, is not fully understood yet. The lowest and the highest energy PL peaks are almost always considerably lower in intensity than the other two; this does not necessarily imply that there is a lower amount of the corresponding material. But a low amount of the corresponding material would explain the low intensity of this peak. Thus, this material might not be percolated and might not contribute to the transport, which is what we measure in QE.

A similar behaviour is observed in the QE spectra reported in the literature: the QE spectra of nominally pure $Cu_2ZnSnSe_4$ extrapolate to a range of different bandgaps: The QE's from Brammertz *et al.*[8] extrapolate to 0.88 eV and 0.94 eV, while the QE from Repins *et al.*[7] extrapolates to 0.90 eV.

Surely, the linear extrapolation of the QE is not the most ideal method to determine the bandgap, but it certainly gives an idea of the absorption edge. For a solar cell absorber which exhibits only one bandgap, different QE would extrapolate to the same bandgap value, as is the case for example in $CuInSe_2$.[46] In the following, we will show that the presence of more than one fundamental bandgap can lead to a continuous change in the apparent bandgap as extrapolated from QE. The quantum efficiency QE near the fundamental bandgap is given by the following formula: $QE \sim 1 - e^{-\alpha L}$, where α denotes the absorption coefficient and L is equal to the effective collection length which is equal to the sum of the space charge region width and the minority carrier diffusion length.[47] We describe the QE spectra by assuming the same collection lengths of the different materials within the sample.

In our model, we assume the presence of two different materials with different bandgaps and absorption spectra. The aim of this simple modeling is to demonstrate the effect that the existence of several bandgaps can have on the observed QE spectra.

The absorption in the model is simulated using the Beer–Lambert's law with the equation

$$A = 1 - e^{df\alpha_1 + d(1-f)\alpha_2}, \quad (1)$$

where f is a parameter representing the fractions of the two simulated materials, d is the thickness of the whole layer (set to 2 μm in the simulation), and $\alpha_{1,2}$ are the absorption coefficients of the two materials. The result of this simulation is shown in Fig. 6.

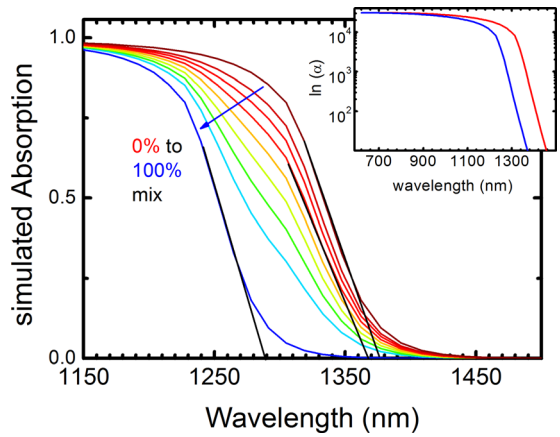

FIG. 6. Simulated absorption of a mix of two materials of 0.9 eV bandgap (red) and 0.96 eV (blue). The black lines show the linear extrapolation to the bandgap of the mix for three absorption curves. The inset shows a logarithmic plot of the two simulated absorption coefficients (using Diplot) for the two materials used for the simulation.

The absorption coefficients are simulated using an optical modelling toolkit in the program Diplot[48] introducing an additional band tailing at low energy (shown in the inset of Fig. 6). The absorption coefficient is modelled by

$$\alpha(E) = \alpha_b \frac{\sqrt{(E - E_G)kT}}{E} + \alpha_U e^{(E-E_1)/E_U}, \qquad (2)$$

where α_b is a parameter set so that the absorption strength is $18\,000\,\mathrm{cm}^{-1}$. α_U and E_1 are parameters that correct the absorption coefficient below the bandgap E_g when an Urbach tailing is simulated. α_U is set to zero at energies above the bandgap E_g. The materials have been simulated with a direct bandgap E_g at 0.9 eV and 0.96 eV, the two extreme values we observe for the bandgap determined from the QE spectra. Both materials are simulated with the same absorption strength and with an Urbach energy (E_U) in the range of 15 meV, which is typical for polycrystalline material.[49] E_1 and α_U are parameters whose only task it is to make the Urbach tail and the band-band part of the absorption a differentiable function. The absorption curves were not fitted to any QE or experimental absorption spectra. We just used reasonable parameters for the two spectra that represent typical absorption spectra in polycrystalline semiconductors with some influence of defect tailing.

The only difference between the two absorption coefficients is that they are shifted in bandgap by 60 meV. The values for the bandgaps are chosen based on the extrapolation of the QE which is in accordance with two of the bandgaps deduced from the intensity dependent RT PL study. The result of this simulation is shown in Fig. 6. When extrapolating the absorption spectra linearly, as we do for the QE spectra, we observe an almost continuous transition from the high energy bandgap to the low energy bandgap. Additionally, it is also seen, that the slope becomes rather shallow for certain mixtures. What we show in Fig. 6 is just the absorption spectrum. The QE spectra increase much slower with decreasing wavelength, since the slope of the QE spectrum also depends on the collection probability. But even the absorption alone without any reduction by non-ideal collection can become shallow with a small fraction of the lower bandgap material. This simulation shows that the presence of two different materials with different bandgaps can lead to an extrapolation of the absorption which results in a continuously changing effective bandgap. Thus, it is possible to explain the observed variation in bandgaps by the presence of different materials with only two different bandgaps. For this simulation, we chose the most conservative approximation: Only two different bandgaps in the absorber are simulated. A more complex simulation with more materials and a larger variety of resulting absorption spectra as implied by the PL measurements will likely lead to a better agreement with the experimental data.

C. Shockley Queisser limit of material mix

The different bandgaps found by room temperature photoluminescence are detrimental to the performance of the resulting solar cell. In an attempt to quantify these losses, the impact of a mix of four semiconductors on the solar cell performance in the ideal SQ limit[50] is therefore investigated. This work is similar to the calculations by Rau *et al*. who calculated the influence of bandgap fluctuations.[51] Here, we consider a fixed number of distinct bandgaps. The worst case, a maximal number of four bandgaps simultaneously seen on one sample is simulated. The simulation is performed for otherwise ideal conditions, namely, the conditions of the Shockley-Queisser model:[50] radiative recombination as determined by black body emission as the only recombination path, i.e., a diode ideality factor of 1, and a QE of 1 for energies above the bandgap.

We calculate the efficiency of 5 different solar cells: four solar cells which consist of a single material with one of the four different bandgaps found in the PL investigations and a fifth cell, which consists of a mix of the four materials. We assume that the materials are mixed in a three dimensional fashion, because this would describe our experimental findings better, as discussed above, than a columnar structure, where the materials are arranged next to each other in the plane of the film, or a layered structure, where the materials are arranged on top of each other.

To calculate the efficiency of each solar cell, we need the short circuit current J_{SC}, the open circuit voltage V_{OC}, and the fill factor FF. The J_{SC} is calculated by integrating the global AM1.5 solar spectrum above the respective bandgap, i.e., assuming a quantum efficiency of 1 for all energies higher than the bandgap. For the cell with the material mix, we use the J_{SC} of the highest bandgap material, since in a 3-dimensional intermixing of different materials, the current has to pass all materials and is limited by the lowest J_{SC}. The open circuit voltage is obtained by rearranging the ideal diode J-V behavior

$$V_{OC} = \frac{kT}{e} \ln\left(\frac{J_{SC}}{J_0} + 1\right). \qquad (3)$$

Thus, to calculate V_{OC}, we need the reverse saturation current J_0 in addition to the short circuit current J_{SC}. J_0 is calculated assuming radiative recombination as the only recombination path, by integrating the black body spectrum of a body at 300 K above the bandgap of each cell.[48] The reverse saturation current of the solar cell with the material mix is calculated as the arithmetic average of saturation currents of the four cells with pure absorbers, since each material can emit its black body radiation in a mixed 3-dimensional arrangement. The V_{OC} of each cell was then calculated according to Eq. (3) with the short circuit current and the reverse saturation current of each cell.

To determine the fill factor of each cell, the $J(V)$ curve is calculated with the ideal diode equation using the respective J_0 and J_{sc} of each cell. The efficiency is calculated from the maximum power point of this calculated ideal diode, which also gives the fill factor.

Fig. 7 summarizes the results of single bandgap solar cells in the SQ limit for the bandgaps seen in the RT PL study as well as the results for a mixed bandgap cell. Fig. 7 shows the solar cell parameters J_0, J_{sc}, V_{oc}, and the efficiency as columns normalized to highest value. The parameters of

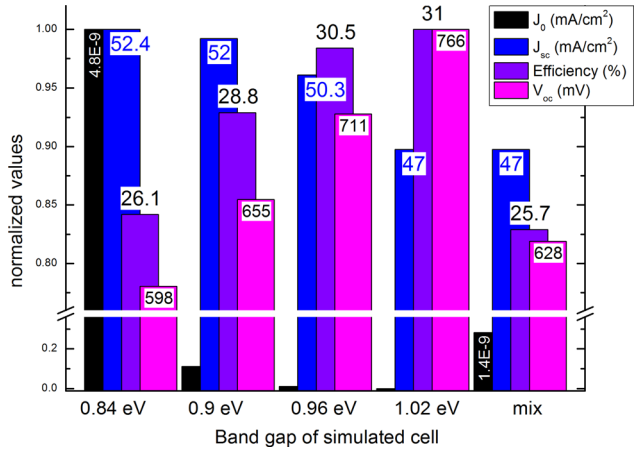

FIG. 7. Solar cell parameters (J_0, J_{sc}, V_{oc}, efficiency) as a function of the bandgap calculated in the Shockley-Queisser conditions. The simulation results for a device with the mix of the four bandgaps is labelled "mix." The highest values of each parameter are normalized to one for a better overview.

the solar cells are shown grouped for each of the bandgaps 0.84 eV, 0.90 eV, 0.96 eV, and 1.02 eV and the mixed bandgap cell. A break in the vertical axis is introduced to visualize the exponentially decaying J_0.

The open circuit voltage of the mix $V_{oc\ mix}$ mainly depends on $J_{0\ mix}$ since J_0 varies over several orders of magnitude (see Fig. 7) as opposed to J_{sc} which varies only within 10% for the considered solar cell. Using the J_{sc} of the lowest bandgap would only increase $V_{oc\,mix}$ by 3 mV. The main result is that the ideal efficiency of the mix (25.7%) is lower than the lowest efficiency of a single bandgap (26.1% with a 0.84 eV bandgap). The $V_{oc\,mix}$ (628 mV) is strongly influenced: it is 138 mV lower than the V_{oc} of the best single bandgap cell and it is lower by 55 meV than the average V_{oc} of the single bandgaps. The same simulation without the lowest bandgap shows, as expected, a less dramatic decrease in the solar cell parameters (i.e., $V_{oc\,mix} = 681$ mV and an efficiency of 28.1%, i.e., a 10% higher efficiency than with the lowest band gap).

These losses, of the mixed bandgap cell compared to a single bandgap cell, are already significant in the ideal case of only radiative recombination. It is expected that the losses due to non-radiative recombination are amplified by the coexistence of multiple materials: for example, the interface area between the 3-dimensionally mixed materials will be large and will likely contribute to enhanced recombination. Additionally, transport barriers are likely to form at the interfaces.

IV. CONCLUSIONS

Room temperature PL of $Cu_2ZnSnSe_4$ often shows several peaks in one sample or different peak energies for different samples.[7,9,31] This is unexpected in a semiconductor with a single bandgap at room temperature. By the use of intensity dependent PL measurements, we found that the highest energy emission, which has previously been attributed to a ZnSe secondary phase, is a defect related transition, in agreement to the previous ascription. In the energy range expected for the bandgap of $Cu_2ZnSnSe_4$, we observe up to four different emissions, which were shown by intensity dependent measurements to be due to band-band transitions. Thus, up to four different materials with different bandgaps are present in the absorber. We can only speculate that there are different polymorphs of $Cu_2ZnSnSe_4$ present, as well as additional secondary phases.

This mixture of materials can explain the different observed bandgap values obtained from extrapolating the QE spectra, as we show in a simple simulation of the absorption spectrum of a thin film containing two different materials with different bandgaps. The presence of different bandgaps within the absorber of a solar cell is detrimental to the efficiency of the solar cell. We simulate the efficiency of a mixed solar cell under the ideal conditions of the SQ model and find that the efficiency is lower than the lowest efficiency of a cell with a single bandgap, where the bandgap energies are taken from energies found in the PL study. It is mostly the open circuit voltage which is affected.

We conclude that all our current $Cu_2ZnSnSe_4$ absorbers contain different polymorphs or secondary phases with different bandgaps, which is detrimental for the efficiency, in particular, for the open circuit voltage of the solar cells. For a further improvement of the efficiency of kesterite solar cells, a control of the different materials with the aim of eliminating low bandgap phases will be essential.

ACKNOWLEDGMENTS

The authors acknowledge the financial support by the Luxembourgish Fonds National de la Recherche.

[1]W. Wang, M. T. Winkler, O. Gunawan, T. Gokmen, T. K. Todorov, Y. Zhu, and D. B. Mitzi, Adv. Energy Mater. **4**, 1301465 (2014).
[2]G. Brammertz, M. Buffière, S. Oueslati, H. ElAnzeery, K. Ben Messaoud, S. Sahayaraj, C. Köble, M. Meuris, and J. Poortmans, Appl. Phys. Lett. **103**(16), 163904 (2013).
[3]A. Chirila, P. Reinhard, F. Pianezzi, P. Bloesch, A. R. Uhl, C. Fella, L. Kranz, D. Keller, C. Gretener, H. Hagendorfer, D. Jaeger, R. Erni, S. Nishiwaki, S. Buecheler, and A. N. Tiwari, Nat. Mater. **12**(12), 1107–1111 (2013).
[4]P. Jackson, D. Hariskos, R. Wuerz, W. Wischmann, and M. Powalla, Phys. Status Solidi RRL **8**(3), 219–222 (2014).
[5]D. Mitzi, O. Gunawan, T. Todorov, K. Wang, and S. Guha, Sol. Energy Mater. Sol. Cells **95**(6), 1421–1436 (2011).
[6]A. Redinger, M. Mousel, M. H. Wolter, N. Valle, and S. Siebentritt, Thin Solid Films **535**, 291–295 (2013).
[7]I. Repins, C. Beall, N. Vora, C. D. Hart, D. Kuciauskas, P. Dippo, B. To, J. Mann, W.-C. Hsu, A. Goodrich, and R. Noufi, Sol. Energy Mater. Sol. Cells **101**, 154–159 (2012).
[8]G. Brammertz, Y. Ren, M. Buffière, S. Mertens, J. Hendrickx, H. Marko, A. E. Zaghi, N. Lenaers, C. Köble, J. Vleugels, M. Meuris, and J. Poortmans, Thin Solid Films **535**, 348 (2013).
[9]B. Shin, Y. Zhu, N. A. Bojarczuk, S. J. Chey, and S. Guha, Appl. Phys. Lett. **101**(5), 053903 (2012).
[10]J. Mattheis, U. Rau, and J. Werner, J. Appl. Phys. **101**(11), 113519 (2007).
[11]A. Redinger, D. M. Berg, P. J. Dale, R. Djemour, L. Gütay, T. Eisenbarth, N. Valle, and S. Siebentritt, J. Photovoltaics **1**(2), 200–206 (2011).
[12]G. Brammertz, M. Buffiere, Y. Mevel, Y. Ren, A. E. Zaghi, N. Lenaers, Y. Mols, C. Koeble, J. Vleugels, M. Meuris, and J. Poortmans, Appl. Phys. Lett. **102**(1), 013902 (2013).
[13]I. V. Dudchak and L. V. Piskach, J. Alloys Compd. **351**(1–2), 145–150 (2003).
[14]S. Chen, X. G. Gong, A. Walsh, and S.-H. Wei, Appl. Phys. Lett. **94**(4), 041903 (2009).
[15]C. Persson, J. Appl. Phys. **107**(5), 053710 (2010).

[16]S. Botti, D. Kammerlander, and M. A. L. Marques, Appl. Phys. Lett. **98**, 241915 (2011).
[17]R. Djemour, M. Mousel, A. Redinger, L. Gütay, A. Crossay, D. Colombara, P. Dale, and S. Siebentritt, Appl. Phys. Lett. **102**, 222108 (2013).
[18]A. Redinger, M. Mousel, R. Djemour, L. Guetay, N. Valle, and S. Siebentritt, Prog. Photovoltaics **22**, 51 (2014).
[19]S. Schorr, Sol. Energy Mater. Sol. Cells **95**(6), 1482–1488 (2011).
[20]D. Dumcenco and Y. Huang, Opt. Mater. **35**(3), 419 (2013).
[21]X. Fontane, V. Izquierdo-Roca, E. Saucedo, S. Schorr, V. O. Yukhymchuk, M. Y. Valakh, A. Perez-Rodriguez, and J. R. Morante, J. Alloys Compd. **539**, 190–194 (2012).
[22]R. Djemour, A. Redinger, M. Mousel, L. Guetay, X. Fontane, V. Izquierdo-Roca, A. Perez-Rodriguez, and S. Siebentritt, Opt. Express **21**(13), A695–A703 (2013).
[23]D. Abou-Ras, T. Kirchartz, and U. Rau, *Advanced Characterization Techniques for Thin Film Solar Cells* (Wiley-VCH, Weinheim, Germany, 2011).
[24]F. Luckert, D. I. Hamilton, M. V. Yakushev, N. S. Beattie, G. Zoppi, M. Moynihan, I. Forbes, A. V. Karotki, A. V. Mudryi, M. Grossberg, J. Krustok, and R. W. Martin, Appl. Phys. Lett. **99**, 062104 (2011).
[25]K. Hoenes, E. Zscherpel, J. J. Scragg, and S. Siebentritt, Phys. B **404**(23–24), 4949–4952 (2009).
[26]T. Schmidt, K. Lischka, and W. Zulehner, Phys. Rev. B **45**(16), 8989–8994 (1992).
[27]J. I. Pankove, *Optical Processes in Semiconductors* (Dover Publications, New York, 1975).
[28]S. Siebentritt and U. Rau, *Wide-Gap Chalcopyrites* (Springer, Berlin, Heidelberg, New York, 2006).
[29]M. Grossberg, J. Krustok, J. Raudoja, and T. Raadik, Appl. Phys. Lett. **101**(10), 102102–102104 (2012).
[30]A. Redinger, D. M. Berg, P. J. Dale, and S. Siebentritt, J. Am. Chem. Soc. **133**, 3320 (2011).
[31]M. Mousel, T. Schwarz, R. Djemour, T. P. Weiss, J. Sendler, J. C. Malaquias, A. Redinger, O. Cojocaru-Mirédin, P.-P. Choi, and S. Siebentritt, Adv. Energy Mater. **4**(2), 1300543 (2014).
[32]R. Scheer and H. W. Schock, *Chalcogenide Photovoltaics: Physics, Technologies, and Thin Film Devices* (Wiley-VCH, 2011).
[33]P. Würfel, *Physics of Solar Cells* (Wiley-VCH, Weinheim, 2005).
[34]P. Würfel, J. Phys. C: Solid State Phys. **15**, 3967–3985 (1982).
[35]S. Siebentritt and S. Schorr, Prog. Photovoltaics **20**, 512–519 (2012).
[36]A. Redinger, K. Hönes, X. Fontané, V. Izquierdo-Roca, E. Saucedo, N. Valle, A. Pérez-Rodríguez, and S. Siebentritt, Appl. Phys. Lett. **98**, 101907 (2011).
[37]S. Ahn, S. Jung, J. Gwak, A. Cho, K. Shin, K. Yoon, D. Park, H. Cheong, and J. H. Yun, Appl. Phys. Lett. **97**(2), 021905 (2010).
[38]M. Grossberg, J. Krustok, K. Timmo, and M. Altosaar, Thin Solid Films **517**, 2489–2492 (2009).
[39]A. M. Hermann and L. Fabick, J. Cryst. Growth **61**(3), 658 (1983).
[40]J. A. Rivet, Ann. Chim. (Paris) **10**, 243 (1965).
[41]G. Marcano, C. Rincon, L. M. de Chalbaud, D. B. Bracho, and G. S. Perez, J. Appl. Phys. **90**, 1847 (2001).
[42]Z. Zainal, A. Kassim, M. Z. Hussein, and C. H. Ching, Mater. Lett. **58**(16), 2199 (2004).
[43]G. S. Babu, Y. B. K. Kumar, Y. B. K. Reddy, and V. S. Raja, Mater. Chem. Phys. **96**(2–3), 442 (2006).
[44]M. Mousel, A. Redinger, R. Djemour, M. Arasimowicz, N. Valle, P. Dale, and S. Siebentritt, Thin Solid Films **535**, 83–87 (2013).
[45]T. Schwarz, O. Cojocaru-Mirédin, P. Choi, M. Mousel, A. Redinger, S. Siebentritt, and D. Raabe, Appl. Phys. Lett. **102**, 042101 (2013).
[46]V. Depredurand, Y. Aida, J. Larsen, A. Majerus, and S. Siebentritt, in *Proceedings of 37th IEEE Photovoltaic Specialist Conference* (IEEE, Seattle, 2011), pp. 337–342.
[47]R. Klenk, H.-W. Schock, and W. H. Bloss, in *Proceeding of 12th European Photovoltaic Solar Energy Conference* (Amsterdam, 1994), Vol. 11, pp. 1588–1591.
[48]E. Lotter, www.diplot.de. (2009).
[49]S. Siebentritt, L. Gütay, D. Regesch, Y. Aida, and V. Deprédurand, Sol. Energy Mater. Sol. Cells **119**, 18 (2013).
[50]W. Shockley and H. J. Queisser, J. Appl. Phys. **32**(3), 510–519 (1961).
[51]U. Rau and J. Werner, Appl. Phys. Lett. **84**, 3735 (2004).